

Fossil earthquakes recorded by pseudotachylytes in mantle peridotite from the Alpine subduction complex of Corsica

Torgeir B. Andersen ^{*}, Håkon Austrheim

Physics of Geological Processes and Department of Geosciences, University of Oslo, P.O.Box 1047, Blindern, 0316 Oslo, Norway

Received 17 March 2005; received in revised form 28 October 2005; accepted 28 November 2005

Available online 10 January 2006

Editor: E. Boyle

Abstract

Paleo-earthquakes recorded by pseudotachylytes have recently been discovered in the blueschist facies subduction complex of Alpine Corsica. Pseudotachylytes occur in ophiolite gabbro and mantle peridotite belonging to the Schistes Lustrés of Cape Corse. Ultramafic pseudotachylyte fault- and injection veins are found within well-preserved peridotite lenses and are progressively hydrated together with the host rock along the margins of the lenses. Numerous pseudotachylytes ranging in thickness from less than 1 to 380 mm have been identified. Veins thicker than 3 mm may show flow banded chilled glassy margins and cores with dendritic to spherulitic quench textures. The newly formed minerals are zoned olivine (Fo_{93–89}), clino- and ortho-pyroxene with compositions indicative of high crystallization temperatures (1300–1400 °C), zoned Cr-spinel, and a glassy to micro-vesicular hydrous matrix showing that frictional melts contained up to 4% water. Frictional heating on co-seismic faults raised the temperature from ambient blueschist facies conditions (450 °C and 1–1.5 GPa) to more than 1700 °C, which is required for ~75% disequilibrium melting of spinel peridotite at 1.5 GPa. The characteristic fault-vein thicknesses observed are 1 to 3 cm, but several fault-veins are thicker than 10 cm. Co-seismic displacement of 1 m, a stress of 300 MPa, and seismic efficiency of 5%, may melt ca 60 kg peridotite pr. m² fault surface corresponding to 20 mm thick layer of ultramafic pseudotachylyte. The ultramafic pseudotachylytes described here formed by disequilibrium melting of peridotite in the upper part of the Alpine subduction zone. If the interpretations of typical displacements of approximately 1 m are correct, the most common pseudotachylyte fault-veins are related to magnitude ca. 7 or larger subduction earthquakes.

© 2005 Elsevier B.V. All rights reserved.

Keywords: subduction; earthquake; mantle; pseudotachylyte; peridotite; Corsica

1. Introduction

Subduction zones are the most seismically active tectonic regime on Earth. A wealth of information regarding the depth distribution of earthquakes has

shown that segments of a subduction zone may change from seismically active to aseismic and that the depth distribution of seismicity may vary between subduction zones and along strike within the same zone. This variation may in some cases relate to age [1] and can be correlated to temperature differences. However, the existing complexity such as double seismic zones [2] makes it obvious that temperature cannot be the only parameter that controls depth distribution. Rocks cycled through subduction zones not only vary in temperature

^{*} Corresponding author. Tel.: +47 22856415; fax: +47 22855101.

E-mail addresses: t.b.andersen@geo.uio.no (T.B. Andersen), hakon.austrheim@geo.uio.no (H. Austrheim).

but also in composition including water content and metamorphic status. This variation may also influence the mechanism and the depth distribution of the seismic activity [3]. Peridotites and their hydrated equivalent serpentinites are dominant rocks in subduction zones as witnessed by their abundance in exposed subduction complexes. These rocks have widely different petro-physical properties and their distribution may influence the location of epicentres. To better understand the mechanism behind subduction earthquakes and their distribution it is required that we understand the physics on the fault planes transecting ultramafic rocks during seismic events. A central question relates to the behaviour of dry peridotite. Is it possible that the high strength and high melting temperature will prevent faulting or is the strength a prerequisite for the build up of stresses to be released as earthquakes?

In this study we describe ultramafic pseudotachylytes recently discovered in mantle peridotites from the Eocene Alpine subduction complex of Corsica [4]. The pseudotachylytes and frictional heating associated with ultra-fine-grained cataclastic rocks suggests that deformation as well as metamorphic transformations at such depths may be associated with short-lived brittle events. Descriptions of ultramafic pseudotachylytes are rare in the literature. We are aware of 3 previously described examples of pseudotachylyte or pseudotachylyte-like veins from peridotites. Obata and Karato [5], followed by Jin et al. [6] documented frictional faulting at high differential stresses (300–600 MPa) resulting in disequilibrium melting of spinel peridotite from the Ivrea–Verbano zone of the Italian Alps. Morishita, [7] and Lund, [8] have provided detailed description and fabric analyses of ultra-fine-grained, fault-related, veins in spinel and garnet peridotite from Hokkaido, Japan and from Holsnøy, western Norway, respectively. The pseudotachylytes described in the present study from Corsica are important because:

- (1) They record paleo-earthquakes in oceanic mantle lithosphere deformed at high-pressure and low-temperature (HP-LT) conditions in a tectonic setting similar to the subduction environment where most of the energy generated by present-day seismic faulting is released [9]. The blueschist facies pseudotachylytes may therefore provide insight into fault-plane processes on subduction earthquakes in the upper parts of Wadati–Benioff zones.
- (2) Disequilibrium melting as shown by a large number of mafic and ultramafic pseudotachylyte veins in rocks with very high melting temperatures

documents that friction on faults is an extremely effective way to transfer elastic energy into heat. These rocks provide an avenue to understand stress-release and the energy budget on deep seismic faults.

- (3) The ultramafic pseudotachylytes are preserved in the least altered and hydrated peridotites and have not been observed in the metamorphically equilibrated serpentinites. Nevertheless the pseudotachylytes preserve evidence that some fluid was available during their formation. Pseudotachylytes and ultra-cataclastites provide an opportunity to study feedback mechanisms between co-seismic slip events and metamorphism, in particular the relationships between frictional heating and dehydration/hydration reactions.

Pseudotachylytes are products of extreme brittle deformation, resulting in comminution and frictional melting at high ($>10^{-2}\text{s}^{-1}$) strain rates [10]. Pseudotachylytes generated by frictional melting in faults commonly occur in crystalline rocks of intermediate and granitoid composition, but may also be derived from gabbroic, and ultramafic protoliths [5,7,11]. Friction on faults may be an efficient heat generating process capable of transferring kinematic energy into frictional heat and give disequilibrium melting of most rock-compositions. On strong faults, by far most of the kinematic energy is transferred to heat. The dynamic coefficient of friction may, however, be greatly reduced when seismic slip velocities are approached [12]. The most effective transfer of kinematic energy to heat, frictional fusion and generation of pseudotachylyte may therefore be most common along fault tips and fracture propagation fronts, and are not necessarily associated with the maximum fault displacements (c.f. [13]). The energy released during faulting (W_f) is mostly dissipated as heat (Q) and depending on the seismic efficiency (η) a very minor component is radiated as seismic energy (E_η):

$$W_f = Q + E_\eta. \quad (1)$$

Although difficult to quantify in general, estimates of (1) suggest that most of the energy ($\approx 95\text{--}99\%$) is transferred to heat [14]. The energy generated by friction in a single seismic event is essentially adiabatic since the heat-transfer-distance (D) into the fracture wall is very small during the seismic event:

$$D = (\kappa t)^{0.5} \quad (\text{thermal diffusivity } \kappa \sim 1.5 \text{ mm}^2\text{s}^{-1}, \\ t - \text{time in sec}). \quad (2)$$

Since the thermal transport in crystalline rocks is extremely inefficient (2) most of the heat will be concentrated in the immediate vicinity (mm to cm) of the fractures. It is therefore to be expected that all fault zones record frictional heating [15]. Some faults, however, do apparently not record detectable frictional heating, and carefully designed studies have failed to document significant increased temperature, and heat-flow measurements in drill-cores from the San Andreas and associated faults in California have also had similar

paradoxical results regarding increased temperatures [16]. Explanations of such observations may include problems with accurate measurements of the temperature, very weak faults with corresponding low normal stresses, dissipation of the heat across wider damage zones, slow deformation and perhaps most importantly advective heat transport by groundwater [17,18]. Many fault zones, however, display dramatic illustrations of how mechanical work has been converted to heat. The most convincing products of frictional heating are pseu-

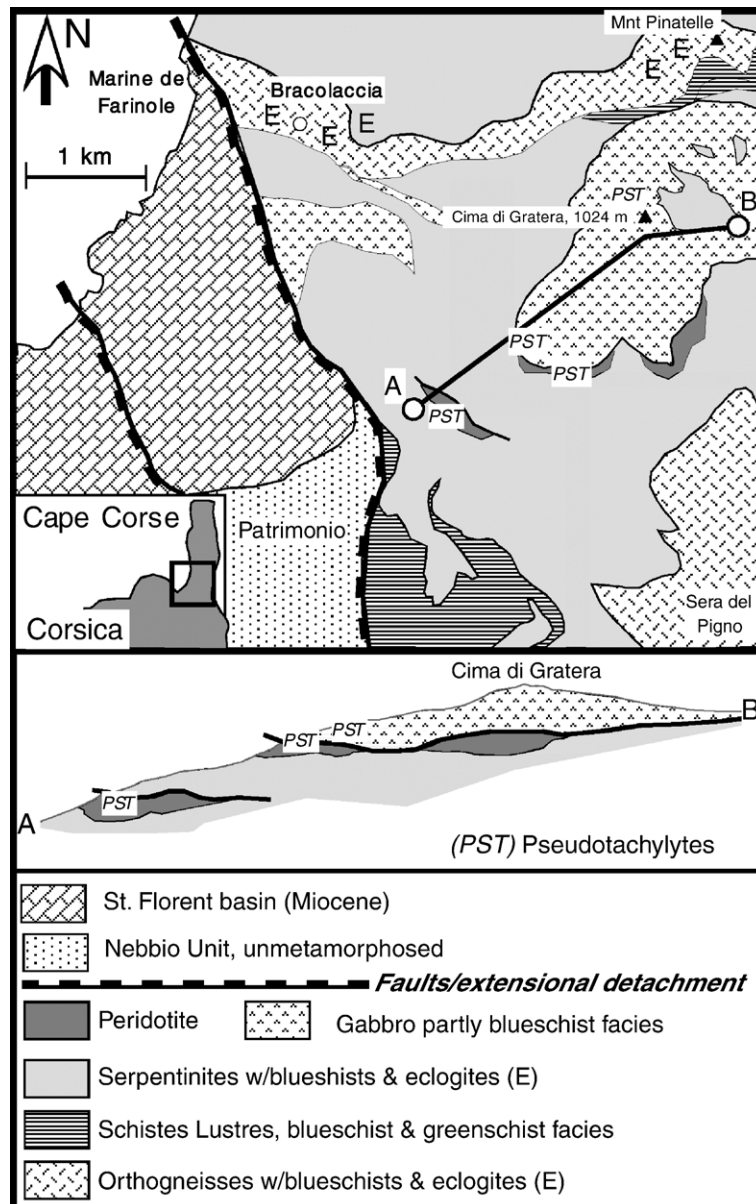


Fig. 1. Simplified geological map and cross-section of the Patrimonio-Cima di Gratera area of the Cape Corse Region, Corsica. Notice that pseudotachylytes are common along the contact between the gabbro and the structurally underlying ultramafic rocks, but also within preserved peridotite lenses preserved within the serpentinite. Most of the detailed observations are from within the lower peridotite body close to A.

dotachylytes such as described in a mostly ignored short paper by Goldschmidt [19], where he interpreted vesicular glass ('frikksjonsglass') along faults in the central Norwegian Caledonides as generated by frictional fusion. Theoretical considerations [20,21] as well as experiments [22], see also review [23] and a large number of studies of natural examples show that frictional heating may result in disequilibrium fusion of the fault wall rocks. Frictional heating associated with large mantle earthquakes will potentially melt any silicate-rock composition from highly silicic to ultramafic [24].

We have recently discovered and described a large number of pseudotachylytes in blueschist to eclogite facies ophiolite gabbro and peridotite of Corsica [25]. The pseudotachylytes in the gabbro and the peridotite are closely associated in space at-or in the vicinity of the gabbro–peridotite contact. Both the mafic and the ultra-mafic pseudotachylytes are precursors of the blueschist facies ductile fabrics in the area, implying

that they are associated in both space and time and therefore related to the same seismic events. These pseudotachylytes are particularly interesting since they provide an opportunity to study the relationships between extreme brittle deformation and the regional HP-LT metamorphism and ductile deformation during burial in a subduction complex [4]. In our pilot study of the pseudotachylytes we documented crystallization and quenching of frictional melts from the Cima di Gratera gabbro (Fig. 1) [25]. The vein/quench mineralogy included minerals such as highly aluminous fassaitic clino-pyroxene, epidote, and edenite-to glaucophane amphiboles suggesting that the seismic faulting and crystallization occurred at a pressure compatible with the regional blueschist facies conditions at ~1 to 1.5 GPa and ca 450 °C. Several previous workers have described and calibrated the blueschist-to eclogite facies metamorphism of the Cape Corse region [26–29], and we take these estimates to represent the ambient

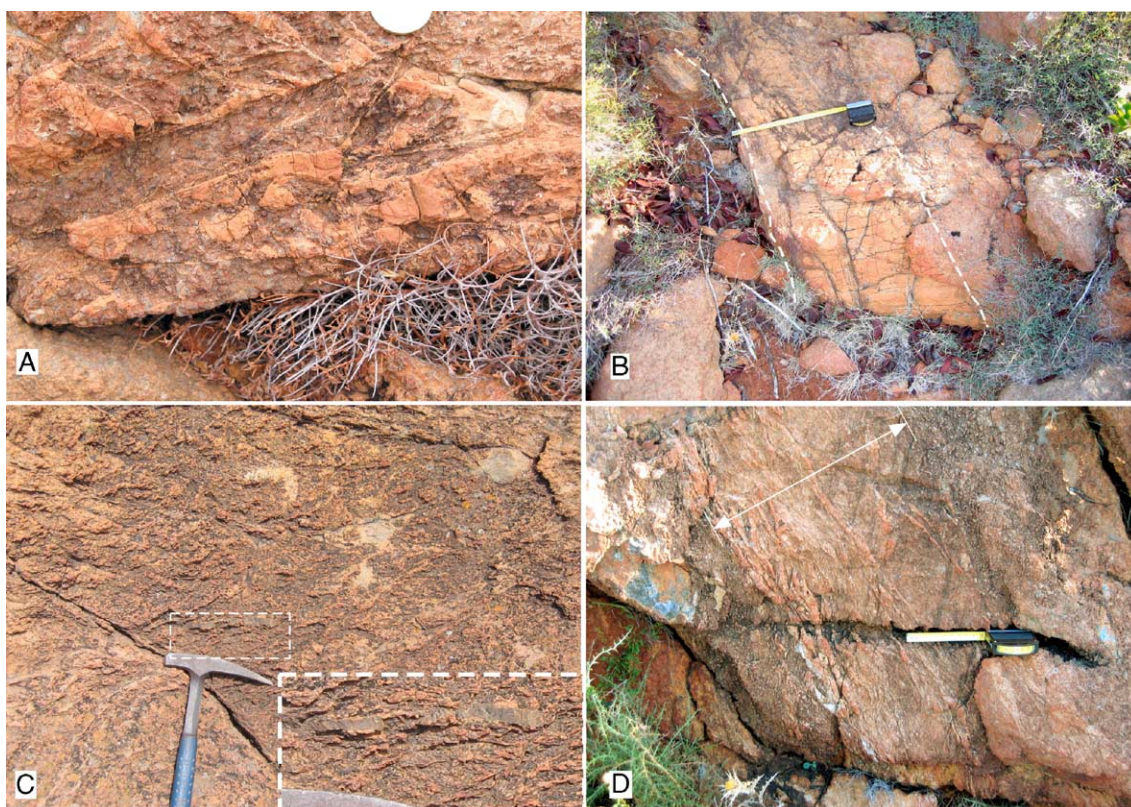


Fig. 2. A) Ultramafic pseudotachylyte fault and injection veins in spinel peridotite. Notice that the veins form positive features on the surface, and that the joints with serpentinisation weather out. Scale: 2-Euro coin. B) Thick segment of pseudotachylyte fault vein with maximum thickness of 38 cm. This fault can be traced almost continuously across the peridotite body (see Fig. 3). The stippled lines show the margins of the fault vein. C) Highly fractured and net-veined fault-core in peridotite along a ca 4.5 m wide fault zone with pseudotachylytes. Framed detail shows well-preserved glassy and unaltered pseudotachylyte vein that may constitute 30% to 40% of the several m-wide damage zone. Locality is near the faulted and sheared contact between upper peridotite (see Fig. 1) and the Cima di Gratera gabbro. D) Fault zone with numerous anastomosing pseudotachylyte veins. Notice the asymmetrical damage zone and that the fault veins are more frequent in the left (lower) part of the fault.

pressure–temperature conditions during the seismic faulting.

2. Geological setting

The studied pseudotachylytes in Corsica occur across a several hundred meter thick section of gabbro and ultramafic rocks within the Schistes Lustrés nappes on the SSW slope of Cima di Gratera at Cape Corse (Fig. 1). The HP-LT complex consists of thrust-stacked units of the Ligurian oceanic lithosphere including plagioclase- and spinel-peridotites imbricated with slices of European continental crystalline rocks with cover [4]. Both the continental and oceanic rocks contain evidence for the late Cretaceous–Oligocene HP-LT metamorphism in the form of blueschists, eclogites and the jadeite-bearing granitoids [28,30,31]. The HP-LT metamorphic rocks include a dismembered ophiolite dominated by variably hydrated and metamorphosed ultramafic rocks, gabbros, pillow lavas and metasedimentary schists (the Schistes Lustrés units). HP-LT metamorphism is also found in allochthonous blueschist (Sera di Pigno and Tenda Units) and eclogite facies (Monte Pinatelle- Farinole Unit) rocks developed from the Hercynian continental basement [4,26,29,32,33]. The eclogites of the Cape Corse Region record peak Alpine metamorphic conditions at pressures of 1.5 to 2 GPa and temperatures of 550 ± 50 °C. They were ex-

humed on a cold geotherm through the blueschist facies at ca 1 GPa and temperatures of 450 to 500 °C and eventually to greenschist facies [26]. Other units, without eclogites reached P_{\max} at lawsonite–blueschist facies (P – 1.3 to 1.5 GPa at T – 350 to 400 °C) and decompressed on a cold geotherm through the blueschist (P – 1 GPa, T – 350 °C) to greenschist facies conditions [26]. The pressure–temperature conditions of blueschist facies rocks of the more external Tenda massif have recently been calculated to T – 300 to 500 °C at P – 0.8 to 1.1 GPa [29]. Previous work in the Cape Corse area suggest that the blueschist to eclogite facies metamorphism was associated with top-to-the-west and southwest Alpine subduction and thrusting, succeeded by the top-to-the-east extension at blueschist to greenschist facies conditions, which eventually juxtaposed the HP-LT rocks with the low-grade to unmetamorphosed Balange and Nebbio units (tectonic summary in [4]).

3. Field description

In outcrop, the ultra-mafic pseudotachylytes form orange to dark brown and occasionally grey to black veins on weathered surfaces and may easily be mistaken for commonly present serpentinite veins. On weathered surfaces they are, however, more resistant and normally define positive features, contrary to most

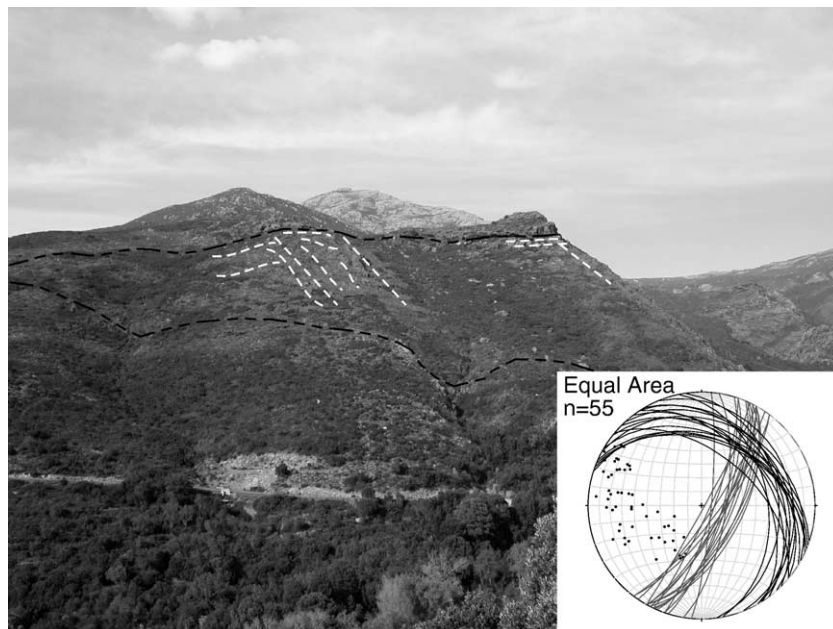


Fig. 3. View showing outline of the lower peridotite body (Fig. 1), between the top and bottom black-dotted lines. Stippled white lines inside the peridotite body show common occurrences and the principal orientations of the pseudotachylytes. The orientation of veins ($n=55$) is shown in the stereogram as poles and great circles. They define a system of mutually crosscutting veins considered to represent a conjugate system.

serpentinite veins, which are softer and weather to form depressions (Fig. 2a). On fresh surfaces they are very dark greenish grey to black aphanitic veins with variable, but usually low content of wall-rock fragments. Flow banding is occasionally visible in hand specimen and commonly observed in thin sections. Most veins are less than 2 cm thick, but occasionally they are much thicker with an observed maximum thickness of 38 cm (Fig. 2b). Hairline-thin veins and fractures are commonly associated with thicker veins (Fig. 2a and c). The weathered surfaces of the wall rocks may be massive and smooth, but more commonly the wall rock surfaces are rough with a fractured appearance formed by better-preserved peridotite cut by abundant small fractures and veins. The pseudotachylytes occasionally occur as single or a few discrete injection veins but more commonly they form networks along faults (Fig. 2). Reconnaissance mapping of pseudotachylytes within two of the peridotite lenses at Cima de Gratera reveal that the veins from which orientations have been measured ($n=55$) can be grouped in two systems. A prominent system comprises laterally consistent and commonly 1–3 cm-thick veins with an average orientation of 025/74 (Fig. 3). A second vein-system dips more gently, is less well oriented but contains some very thick (5–20 cm) fault veins. Near the upper contacts of both peridotite lenses there are continuous and thicker fault-veins that are sub-parallel with the contacts to the serpentinite (lower peridotite) and the blueschist facies foliation in the Cima di Gratera gabbro (upper peridotite, see Fig. 1). Some fault veins are part of systems that can be traced laterally for several meters to several tens of meters, and in one case across most of the lower peridotite body (Fig. 3). A characteristic feature of individual faults with pseudotachylyte veins is that they form an anastomosing network where individual veins may vary in thickness from mm up to a maximum observed width of 38 cm (Fig. 2). The observation of thickness variations by as much as 2-orders of magnitude along the same fault zone suggest that the fault vein thicknesses are commonly secondary, reduced by drainage and thickened by injection into releasing-bend pull-apart segments. These observations indicate that relating fault-vein thicknesses directly to fault displacement [13,21] should be used with considerable caution, since the width of individual pseudotachylyte veins on faults in many cases probably are secondary. In spite of the uncertainty of relating fault vein-thicknesses to displacement we have used the observed characteristic fault vein thickness of ca 2 cm because we lack other accurate displacement indicators for the principal faults (see discussion below). The

peridotite wall rocks are mostly without obvious stratification or banding. Attempts to determine throw or in some cases even relative movement along the continuous faults are therefore difficult. In some cases veins occur within damage-zones that are several meters (max 5 m) wide. The geometry and distribution of fault- and injection veins suggest that the faults constitute a conjugate system accompanied by mode-1 fractures.

Both field- and thin section observations show that the brittle faulting generating pseudotachylytes in general was a precursor of the ductile deformation (Fig. 4b). The pseudotachylyte veins are deformed into the ductile fabric engulfing the lenses. Crosscutting pseu-

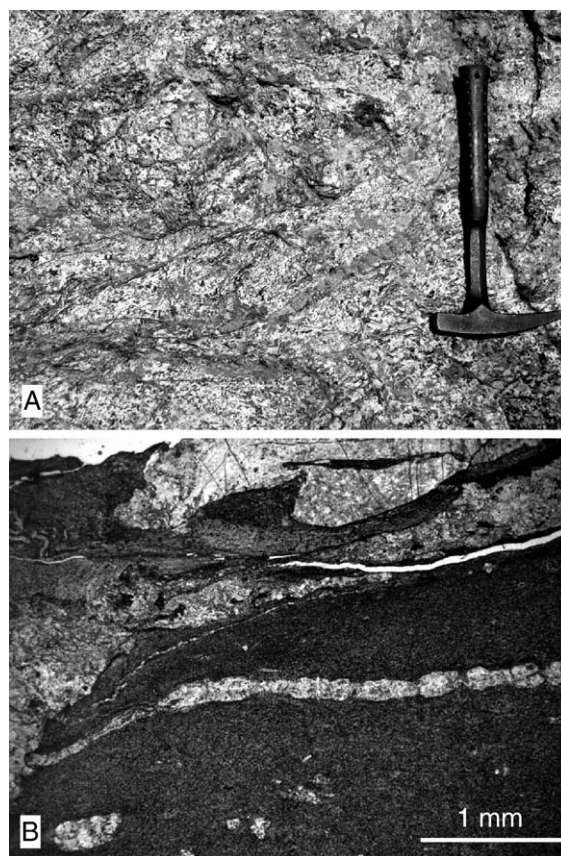


Fig. 4. A) Pseudotachylyte veins in gabbro near the sheared contact to the upper peridotite and serpentinite at Cima di Gratera (see Fig. 1). Notice the well-preserved igneous texture between the fractures and fault/injection veins within the gabbro. B) Optical micrograph (parallel light) of fine-grained blueschist facies deformation zone developed in gabbro near at the contact between mafic and ultramafic rocks at Cima di Gratera. Small glaucophane crystals, (10–30 μm , not visible at this magnification), define a foliation of the fine-grained fault rock. Notice the intrusive features (veins and horn) of the ultrafine-grained margin of the fault rock, suggesting that the fault-rock intruded the wall rock. Notice also pinch and swell of the light-coloured vein (see text for discussion of brittle–ductile relationships).

dotachylytes indicating multiple seismic events along the same faults are commonly observed (see also [25]). Alteration of extreme brittle deformation and creep is witnessed by pseudotachylytes overprinted by ductile fabrics, which in turn are truncated by new fault and/or injections veins (Fig. 5f). Pseudotachylytes truncated by fractures associated with serpentinisation are common on all scales. Pseudotachylytes are, however, only preserved within the least altered peridotite lenses,

which are engulfed within foliated serpentinites and metamorphically more equilibrated rocks. The large seismic events can thus be related to the earlier and driest parts of the structural and metamorphic history. This pattern is akin to brittle–ductile relationships in other HP-LT metamorphic terrains such as the relative timing of eclogite facies pseudotachylytes and shear zones in western Norway [8,34–36]. Once the strength of the peridotites and gabbros become sufficiently re-

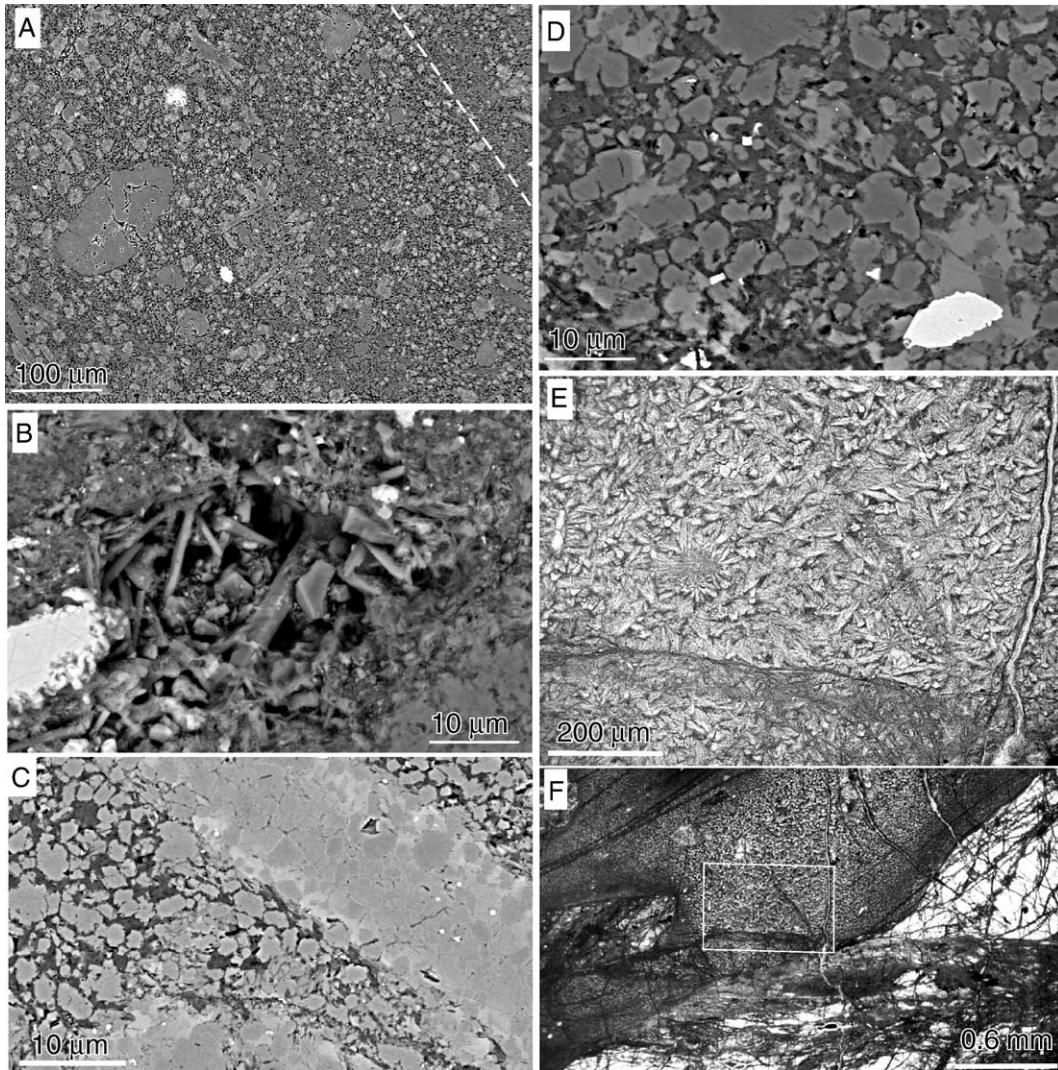


Fig. 5. A) Backscatter-electron (BSE) image of ultramafic pseudotachylyte with flow-banding (parallel dotted line), thermally rounded ol clasts and newly formed ol, opx and cpx (light grey) crystals in darker glassy to fibrous hydrous matrix. The cpx crystals form dendritic to acicular poikilitic crystals. Ol and opx are undistinguishable on the BSE images. Mineral abbreviations after [47] B) BSE image showing vesicle with idiomorphic cpx crystals in ultramafic pseudotachylyte. Light mineral (left) is Cr-spl. C) BSE image showing detail of acicular cpx micro-phenocrysts (light) with abundant (<5-micron) ol inclusions. Notice also chemical zoning, Fe-rim to Mg-core (darker) in the small ol crystals. D) BSE detail showing zoned ol, opx, poikilitic cpx, zoned spl and the micro-vesicular and fibrous hydrous matrix. E) Optical micrograph (parallel light) showing quench texture with spherulitic (sunflower-like) and acicular/dendritic cpx phenocrysts in ultramafic pseudotachylyte. F) Optical micrograph showing quenched pseudotachylyte with micro-phenocrystic core and chilled margin. The vein cuts an older pseudotachylyte with ductile overprint (lower part of photo). The framed area is shown in detail in Fig. 5E.

duced, primarily controlled by hydration of olivine and pyroxenes, crystal–plastic deformation mechanisms and ductile flow dominate and in turn enhance recrystallization and equilibration of tectonites.

The relationships between the pseudotachylyte in peridotite lenses and the foliated serpentinites can be studied along the margins of the lenses. The best-studied peridotite body has a width–thickness ratio of ca 1 to 6 and a maximum thickness ca 100 m. The upper contact is marked by a sharp front of alteration and intense foliation forming a break in the topography (Fig. 3). The lower boundary is less pronounced and less well exposed, with a transition from peridotite to completely hydrated serpentinite over a distance of a few meters. The pseudotachylytes near the contacts are overprinted to obliterated by ductile deformation associated with serpentinisation. Very fine-grained fault-rocks, ultra-cataclastites or former pseudotachylytes, are also overprinted by ductile deformation along the tectonic contact between the Cima di Gratera gabbro and the underlying ultramafic rocks (Fig. 1). Locally the gabbro contains spectacularly preserved pseudotachylytes along this contact ([25] and Fig. 4a). Ductile fabric overprinting former pseudotachylyte or ultra-cataclastite characterizes fine-grained blue mylonites from the contact zone. Well-oriented, small crystals (~0.1 mm) of glaucophane define a CPO fabric in the mylonite (Fig. 4b).

4. Solidification, mineralogy and texture

The ultramafic pseudotachylytes are dark glassy veins, which sharply crosscut individual mineral grains, older veins or deformation zones in the peridotite wall rock. Thin sections reveal that many veins are hairline-thin and difficult to see in the field. Very thin injection veins and grain-boundary wetting-like features require extremely low viscosity for the melt. High-pressure experiments show that ultramafic melts (komatiites and pyroxenites) have very low viscosities of 10^{-1} Pa s or less [37]. Such low viscosity is consistent with the intrusive features associated with the mm-thin ultramafic pseudotachylytes. The mm- to cm-thin veins must have been emplaced and solidified in seconds and ca 10–15 min respectively according to Eq. (3).

$$t_s = b^2 / 4\kappa\lambda^2, \quad (3)$$

where t_s — time for solidification, b — vein thickness in mm, κ — thermal diffusivity ($\sim 1.5 \text{ mm}^2 \text{ s}^{-1}$), $\lambda \sim 0.45$, a dimensionless variable depending on the latent heat

of fusion ($8.6 \times 10^5 \text{ J kg}^{-1}$), heat capacity ($1150 \text{ J kg}^{-1} \text{ }^\circ\text{C}^{-1}$) and temperature difference ($>1200 \text{ }^\circ\text{C}$) between melt and wall rock (see [38] for derivation of Eq. (3)).

Most of the sampled veins are texturally zoned, commonly with ultra-fine grained, colour banded glassy margins and a banding defined by variable content of porphyroclasts. In the best-developed pseudotachylytes, the porphyroclasts are dominated by thermally rounded olivine and minor ortho-pyroxene (Fig. 5a). Veins thicker than 2–3 mm may contain micro-porphyrific domains, mainly in the cores. The micro-phenocrysts are clino-pyroxene crystallized directly from the frictional melt. Other minerals crystallized from the melt include olivine, ortho-pyroxene, chrome-spinel, and nickel-sulphide. Combined optical microscopy, backscatter electron images (BSE) and X-ray element mapping on scanning electron microscope (SEM) and electron microprobe (EMP) analyses show that the minerals which crystallized are small, commonly less than 10 μm , zoned crystals of olivine ($\text{Fo}_{89.0-93.9}$), ortho-pyroxene ($\text{Wo}_{11.7-3.0}$, $\text{En}_{87.3-77.4}$, $\text{Fs}_{14.2-9.6}$) and up to 300 μm long dendritic, spherulitic to acicular clino-pyroxene ($\text{Wo}_{38.9-24.3}$, $\text{En}_{65.4-53.0}$, $\text{Fs}_{10.3-7.1}$) microliths (Table 1 and Fig. 5c and d). The olivine crystals are consistently zoned with Mg-rich cores (Fo_{93}) and more Fe-rich margins (Fo_{89}). The clino-pyroxene crystals are strongly poikilitic to dendritic and may contain more than 80% olivine inclusions in their cores (Fig. 5c, d and e). Pyroxene compositions from crystallites that crystallized from the pseudotachylyte melt, as well as the average wall-rock pyroxene compositions are shown in Fig. 6a. The extreme composition of both ortho- and clino-pyroxene require crystallization temperatures in the range of 1300 to 1400 $^\circ\text{C}$ at a pressure of 1 to 1.5 GPa, in accordance with the ambient blueschist-to eclogite facies pressure conditions [39]. Olivine crystallites in pseudotachylyte also have unusual composition, particularly a high content of CaO compared to the wall rock mineral composition (Fig. 6b).

The interstitial matrix contains small idiomorphic to sub-idiomorphic chromite, chrome spinel and occasional Ni-sulphide crystals ($\sim 1-2 \mu\text{m}$), and larger chrome-spinel crystals, which may be chemically zoned. The zoned spinel crystals have slightly higher average atomic number along the rims (Fig. 5b). These crystals may be up to 10 μm across and may represent spinel porphyroclasts with a Fe-rich rim overgrowth. Veins thinner than ~ 2 mm are generally without the micro-porphyrific texture, but commonly have flow foliation and folding.

Table 1
Mineral composition from Ultramafic pseudotachylytes and wall-rock peridotite, Corsica

PST ol																										
													Zoned ol crystallite			Wall rock olivine										
Sample	Cor9-3	Cor9-3	Cor9-3	Cor9-3	Cor9-3	Cor9-3	Cor9-3	Cor9-3	Cor9-3	Cor9-3	Cor9-3	Average	ol core	ol inter	ol margin	Cor10-03	Cor10-03	Cor10-03	Cor10-03	Cor10-03	Average	Cor11-03	Cor11-03	Cor11-03	Average	
SiO ₂	40.66	41.33	41.55	42.49	41.85	40.77	40.53	40.18	40.82	40.55	40.18	39.93	40.90	42.34	41.58	41.71	40.53	40.82	40.63	40.98	40.86	40.76	41.53	40.91	40.95	41.13
Na ₂ O	0.00	0.00	0.00	0.00	0.00	0.00	0.00	0.00	0.00	0.00	0.00	0.00	0.00	0.00	0.00	0.00	0.00	0.00	0.04	0.00	0.00	0.01	0.00	0.03	0.00	0.01
NiO	nd	nd	nd	nd	nd	nd	nd	nd	nd	nd	nd	nd	nd	0.40	0.34	0.33	nd	nd	nd	nd	nd	0.39	0.03	0.32	0.25	
MgO	49.10	50.60	49.62	47.27	47.11	48.85	48.96	49.16	48.06	48.48	48.88	49.02	48.76	51.95	48.98	48.02	49.09	49.06	48.98	48.93	48.74	48.96	49.42	45.68	48.40	47.83
Al ₂ O ₃	0.09	0.08	0.09	0.29	0.64	0.31	0.00	0.00	0.02	0.01	0.00	0.01	0.13	0.00	0.03	0.12	0.02	0.01	0.03	0.00	0.00	0.01	0.00	0.01	0.00	0.00
K ₂ O	0.00	0.00	0.00	0.00	0.01	0.01	0.02	0.00	0.00	0.03	0.00	0.00	0.01	0.00	0.00	0.00	0.00	0.00	0.00	0.00	0.00	0.00	0.00	0.00	0.02	0.01
CaO	0.22	0.15	0.20	0.99	0.95	0.66	0.01	0.00	0.04	0.41	0.03	0.00	0.30	0.13	0.05	0.10	0.04	0.04	0.11	0.01	0.06	0.05	0.03	0.14	0.03	0.07
TiO ₂	0.05	0.04	0.00	0.03	0.04	0.01	0.00	0.01	0.01	0.00	0.03	0.01	0.02	0.02	0.00	0.00	0.00	0.00	0.01	0.02	0.01	0.01	0.01	0.01	0.01	0.01
Cr ₂ O ₃	0.20	0.23	0.29	0.20	0.26	0.26	0.00	0.02	0.00	0.06	0.00	0.03	0.13	0.18	0.07	0.17	0.02	0.01	0.05	0.00	0.00	0.02	0.00	0.00	0.00	0.00
MnO	0.14	0.11	0.10	0.15	0.12	0.11	0.13	0.11	0.18	0.16	0.12	0.13	0.13	0.07	0.20	0.14	0.12	0.15	0.14	0.20	0.13	0.15	0.13	0.35	0.14	0.21
FeO	9.56	7.79	7.98	9.33	9.28	8.19	9.97	10.32	10.55	10.48	10.62	10.87	9.58	5.93	10.51	10.36	9.91	9.84	9.57	10.05	10.01	9.88	10.39	14.06	11.17	11.87
Total	100.02	100.33	99.83	100.75	100.26	99.18	99.62	99.80	99.68	100.17	99.86	100.00	99.96	101.02	101.76	100.95	99.73	99.93	99.56	100.19	99.81	99.84	101.90	101.22	101.04	101.39
Fo	90.02	91.95	91.63	89.89	89.93	91.30	89.63	89.36	88.87	89.04	89.03	88.82	89.96	93.92	89.07	89.07						89.55	89.33	84.96	88.41	87.57
Fa	9.83	7.94	8.27	9.95	9.94	8.59	10.24	10.52	10.94	10.80	10.85	11.05	9.91	6.01	10.72	10.78						10.32	10.53	14.67	11.44	12.21

PST cpx																										
													PST opx				Wall rock cpx					Wall rock opx				
Sample	cor11	cor11#6	cor11#7	Cor6#19	Cor6#26	#29	#34	Average	Cor11#9	#21	#24	Cor6#22	Cor6#24	Cor6#25	Average	Cor10#6	Cor10#7	Cor10#5	Cor10#4	Average	Cor10#8	Cor10#10	Cor10#9	Cor10#17	Average	
SiO ₂	52.11	54.91	52.38	53.68	52.47	52.01	51.69	52.75	56.52	54.94	54.15	54.80	56.93	56.20	55.20	51.17	50.86	51.38	51.08	51.12	54.27	54.81	54.72	53.16	54.24	
Na ₂ O	0.00	0.02	0.05	0.01	0.06	0.00	0.00	0.02	0.00	0.00	0.00	0.00	0.01	0.04	0.00	0.16	0.09	0.12	0.24	0.15	0.01	0.02	0.00	0.00	0.01	
NiO	nd	0.10	0.11	0.09	0.11	nd	nd	0.10	0.06	nd	nd	0.16	0.17	0.11	0.06	0.12	0.05	0.01	0.00	0.05	nd	nd	nd	nd	nd	
MgO	20.60	23.29	20.40	20.71	18.94	22.53	24.14	21.52	31.88	34.36	29.44	35.09	32.92	32.63	31.89	17.46	17.36	17.36	17.00	17.30	32.59	32.47	32.40	32.05	32.38	
Al ₂ O ₃	3.22	2.32	3.64	3.12	4.02	3.07	3.84	3.32	1.46	1.41	1.81	0.70	2.05	1.95	1.56	3.41	3.41	3.51	3.23	3.39	2.56	2.64	2.57	4.87	3.16	
K ₂ O	0.02	0.00	0.01	0.00	0.00	0.02	0.00	0.01	0.00	0.00	0.00	0.00	0.00	0.01	0.00	0.01	0.01	0.02	0.00	0.01	0.01	0.00	0.01	0.00	0.01	
CaO	17.55	13.94	16.61	18.11	19.35	15.03	12.48	16.15	3.13	1.66	6.17	2.83	1.84	2.35	3.65	22.62	22.61	22.43	22.87	22.63	1.36	1.47	1.35	1.03	1.30	
TiO ₂	0.12	0.11	0.24	0.13	0.18	0.18	0.20	0.17	0.02	0.02	0.04	0.00	0.03	0.02	0.03	0.36	0.35	0.34	0.32	0.34	0.19	0.18	0.16	0.11	0.16	

Cr ₂ O ₃	1.03	0.63	0.53	0.71	0.97	0.66	0.39	0.70	1.19	1.12	0.92	0.72	1.57	1.43	1.08	1.20	1.14	1.19	1.05	1.15	0.77	0.74	0.69	1.01	0.80	
MnO	0.14	0.16	0.14	0.16	0.12	0.13	0.15	0.14	0.15	0.13	0.18	0.17	0.11	0.17	0.15	0.09	0.16	0.12	0.10	0.12	0.14	0.16	0.13	0.15	0.15	
FeO	5.70	5.96	6.05	4.43	4.94	5.72	6.66	5.64	6.68	6.70	7.27	6.73	6.04	6.42	6.88	3.28	3.18	3.17	3.21	3.21	6.70	6.83	6.94	6.94	6.85	
Total	100.49	101.44	100.16	101.15	101.16	99.35	99.54	100.47	101.09	100.32	99.99	101.20	101.67	101.33	100.47	99.88	99.22	99.65	99.10	99.46	98.60	99.32	98.97	99.32	99.05	
Wo	34.58	27.24	33.28	35.84	38.89	29.52	24.31	31.95	5.93	3.03	11.66		5.14	4.44	6.87										2.51	
En	56.58	63.34	56.88	57.04	52.97	61.58	65.43	59.12	83.98	87.33	77.43		80.55	85.73	82.91											86.95
Fs	8.93	9.34	9.65	7.09	7.92	8.90	10.26	8.87	10.09	9.64	10.91		14.26	9.71	10.92											10.51

Low total glassy/fibrous PST matrix

Sample	PST matrix																Srp vein				Cr spl		Wall rock pl			
	cor11#10	cor11#11	#23	#7	#9	#18	#8	#7	#8	#9	cor11#10	cor11#11	cor11-#12	cor11#13	cor11#14	Average	Cor10	Cor11	Cor10	Average	Cor10	Cor10	Cor10	Cor10	Cor10	
SiO ₂	42.35	40.42	42.29	42.35	40.17	37.16	40.43	42.96	41.24	41.53	50.57	53.39	46.52	41.31	38.72	42.76	40.89	40.16	40.96	40.67	0.01	0.00		44.40	44.51	44.78
SrO	nd	nd	nd	nd	nd	nd	nd	nd	nd	nd	nd	nd	nd	nd	nd	nd	nd	nd	nd	nd	nd	nd	nd	nd	nd	nd
BaO	nd	nd	nd	nd	nd	nd	nd	nd	nd	nd	nd	nd	nd	nd	nd	nd	nd	nd	nd	nd	nd	nd	nd	nd	nd	nd
Na ₂ O	0.36	0.18	0.09	0.37	0.02	0.02	0.19	0.00	0.00	0.00	0.43	0.76	0.26	0.00	0.00	0.18	0.00	0.01	0.00	0.00	0.00	0.00	0.00	0.70	0.69	0.66
NiO	0.12	0.05	0.34	0.12	0.09	0.10	0.06	nd	nd	nd	nd	nd	nd	nd	nd	0.13	nd	0.09	nd	nd	nd	nd	nd	nd	nd	nd
MgO	35.71	36.51	42.55	35.72	38.66	35.28	36.51	40.98	38.20	38.08	28.17	25.00	31.81	36.41	38.21	35.85	37.99	38.65	37.68	38.11	11.34	10.83		0.05	0.07	0.09
Al ₂ O ₃	8.89	8.99	1.19	8.90	1.05	11.92	8.99	1.06	3.46	2.80	3.04	2.98	4.49	6.99	7.23	5.46	2.30	1.04	2.65	2.00	25.41	24.59		34.91	35.19	34.93
K ₂ O	0.08	0.04	0.04	0.08	0.00	0.02	0.04	0.02	0.02	0.01	0.01	0.03	0.03	0.02	0.00	0.03	0.02	0.00	0.00	0.01	0.00	0.00		0.00	0.00	0.00
CaO	0.03	0.08	0.64	0.04	0.19	0.10	0.08	1.44	0.18	0.88	7.91	10.27	4.57	1.60	0.06	1.87	0.05	0.19	0.02	0.09	0.02	0.01		19.41	19.66	19.52
TiO ₂	0.04	0.00	0.02	0.04	0.01	0.00	0.00	0.03	0.02	0.03	0.12	0.12	0.08	0.02	0.01	0.03	0.01	0.00	0.00	0.00	0.35	0.38		0.04	0.02	0.00
Cr ₂ O ₃	0.05	0.08	0.92	0.06	0.06	1.64	0.09	0.25	0.47	0.30	0.19	0.10	0.12	0.20	0.24	0.32	0.04	0.06	0.00	0.03	37.11	37.99		nd	nd	nd
MnO	0.03	0.01	0.12	0.03	0.09	0.01	0.02	0.09	0.04	0.02	0.09	0.08	0.06	0.03	0.02	0.05	0.15	0.09	0.09	0.11	0.20	0.24		0.01	0.00	0.00
FeO	2.77	3.22	8.11	2.77	10.05	3.49	3.23	6.83	3.63	3.14	3.37	3.43	3.30	3.08	2.97	4.23	3.90	10.05	3.81	5.92	23.51	24.15		0.24	0.25	0.21
Total	90.43	89.58	96.32	90.48	90.38	89.74	89.63	93.65	87.26	86.80	93.90	96.15	91.23	89.67	87.46	90.84	85.35	90.34	85.21	86.97	97.95	98.19		99.96	100.61	100.23
																							An	94.00	94.00	94.00

Representative electron microprobe analyses (UCSB and UiO) of glassy to fibrous matrix (low-totals) and micro-phenocrysts (ol, opx, cpx, Cr-spl) from the ultramafic pseudotachylytes (PST), srp from serpentine vein, and magmatic minerals (ol, opx, cpx, pl) from wall-rock peridotite. Solid-solution end-member contents are shown for minerals with significant compositional variation. Mineral abbreviations are after [47].

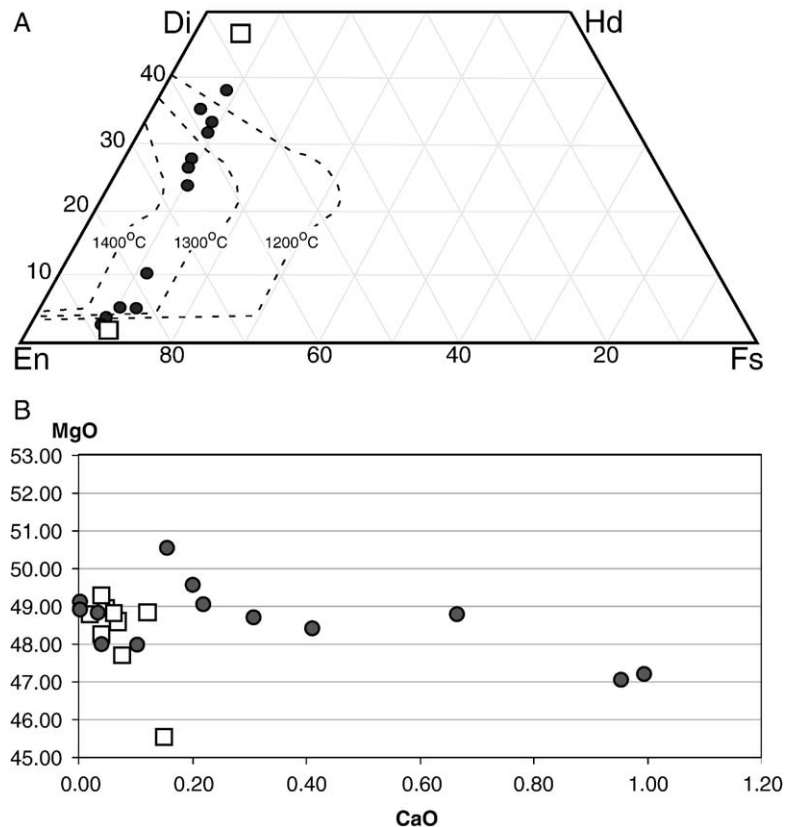


Fig. 6. A) Pyroxene compositions from peridotite wall rock (squares) and from ultramafic pseudotachylyte micro-crystals (circles). Isotherms are from [37]. See text for discussion. B) MgO–CaO composition of ol from pseudotachylyte micro-crystals (circles) and from the wall-rock peridotite (squares) showing high content of CaO in ol from the pseudotachylyte.

BSE images show that the interstitial matrix between porphyroclasts and new-formed crystallites has a low average atomic weight. EMP analyses give a range of ultramafic compositions with SiO₂ and MgO contents from 37.2% to 53.4% and 25% to 42.5%, respectively. The analyses give low totals ranging from 86.8% to 96.5% (see Table 1). Variations between individual nearby analyses points are, however, difficult to reconcile with real mineral compositional variations. We therefore interpret the analyses to represent mixed, non-stoichiometric data and not to represent well-defined individual serpentine crystals. This is supported by the BSE images, which show that the matrix may be glassy homogeneous- to micro-fibrous and micro-porous. Cavities are normally smaller than 1 μm across. In one sample (Cor7b-03), however, a few larger cavities up to 20 μm across have been observed. These probably represent vesicles present at the melt stage since idiomorphic clino-pyroxene crystals have crystallized into the cavity (Fig. 5b). The presence of a micro-vesicular interstitial matrix suggests that the frictional melting was accompanied by high fluid-pressures, which at

least locally was sufficient to release a free gas phase from the melt. The fibrous domains of the matrix probably formed by devitrification of original glass to serpentine, whereas the homogenous domains may be sub-micron scale mineral intergrowths or possibly still glass.

5. Conditions for formation of ultramafic pseudotachylyte

The texture and mineralogy described above show that the pseudotachylyte veins formed by near complete melting of the wall rock composed of olivine (Fo_{87–90}), *ortho*-pyroxene (En₈₇), diopside-rich clino-pyroxene (Wo₄₆, En₄₉, Fs₅) and Cr-rich spinel. Some studied samples also contain minor plagioclase (An₉₄), and all samples have alteration represented by grain-boundary fringes, veins and fracture networks of serpentine. The pseudotachylytes contain small, variably idiomorphic to sub-idiomorphic zoned olivine grains (~10–15 μm) with Mg-rich cores and higher Fe-content along the margins (see above). The compositional range of ana-

lyzed wall rock olivine crystals is more restricted (Fo_{87-90}). The small olivine crystals in the pseudotachylyte also have higher Cr_2O_3 , Al_2O_3 and considerably higher CaO contents than the wall rock olivine (Fig. 6b). We interpret them to be micro-phenocrysts crystallized directly from the friction melt. The zoning patterns as well as the compositional variations between the wall rock and the pseudotachylyte minerals are very similar to the pseudotachylyte described from the Balmuccia peridotite [5]. The pseudotachylyte pyroxenes have extreme compositional variation and reduced opx–cpx immiscibility indicative of high-temperature crystallization (Fig. 6, Table 1, and [39]).

The micro-vesicles observed with SEM (see above) and the low-total-oxide analyses (~90%) of the interstitial matrix suggest that the melt had a high fluid-content and that the melt became fluid-saturated as the water-free micro-phenocrysts formed. Image analyses (Matlab script, written com., Dani Schmid, 2004) from two high-magnification SEM micrographs show that typical pseudotachylyte is composed of 56.4% to 59.2% crystals (ol, cpx, opx, opaques), 39.4% to 41.6% matrix and 1.4% to 2.0% micro-porosity interpreted to represent vesicles (Fig. 5b). The preservation of the primary texture and mineralogy of the micro-phenocrysts suggest that the fluid was originally dissolved in the melt and that the matrix was not hydrated by introduced water at a later stage. The original peridotite must therefore have had an appreciable content of water before it melted by frictional heating. Based on the fluid content of the matrix (low total analyses and micro-porosity) the friction melt contained approximately 12% by volume of a hydrous fluid, or close to 4% by weight assuming an ultramafic melt with density of 2.85 [40]. Experiments and theoretical estimates of water-saturation in a melt at 1 GPa give 13% water by weight [41,42].

The fluid-composition in the studied rocks was most likely dominated by water since carbonates have not been identified in our thin sections. Idiomorphic diopside crystals in vesicles suggest that clino-pyroxene crystals grew after vesiculation (Fig. 5b). Assuming a H_2O fluid content of 4 wt.%, a pressure of 1 to 1.5 GPa as suggested by the ambient blueschist facies regional metamorphic conditions, solidification of the pseudotachylyte melts may have occurred at ca 1200 °C [42]. Based on these observations and the published experimental and theoretical parameterization of peridotite melting by Katz et al. [42], we estimate that friction on the co-seismic faults producing pseudotachylytes in the peridotite must have raised the temperature from the ambient metamorphic conditions of 400 to 450 °C by at

least 1250 °C (δT in Eq. (4)) to a melting temperature of 1650–1700 °C or more.

Paleopiezometry from studies of grain-size and dislocation density (4 to $5 \times 10^{13} \text{m}^{-2}$) in olivine associated with pseudotachylyte in peridotite, compared with experimental results, indicate that peridotites may sustain extreme differential stresses of ca 3–600 MPa [5,6]. We have not been able to measure exact displacement on the studied main faults in the field because well-defined, offset markers have not been identified. However, if we assume that there is a characteristic relationships between energy per m^2 fault surface and the volume of melted peridotite, and that fault veins with consistent pseudotachylyte thicknesses represent faults with a minimal leakage of melt into the wall-rocks or releasing bends, we can use the volume of melt to estimate displacement [13]. A magnitude ~7 earthquake with displacement $d \sim 1$ m [43] and a differential stress of 300 MPa in mantle peridotite [5] will release energy according to Eq. (1): $W_f = Q + E_\eta$; which is equal to: $W_f = d \times \sigma_n = d \times (\sigma_1 - \sigma_3) / 2 = 1 \text{ m} \times (300 \text{ MPa}) / 2 \approx 1.5 \times 10^8 \text{ Jm}^{-2}$. If the seismic efficiency (η) is ~5%, the radiated seismic energy E_η is $7.5 \times 10^6 \text{ Jm}^{-2}$, the remaining energy ($Q = 1.425 \times 10^8 \text{ Jm}^{-2}$) turns to heat and surface energy along the fault. The process is adiabatic since the fault movement occurs in seconds and no heat is lost by conduction (thermal diffusivity $\kappa \sim 1.5 \text{ mm}^2 \text{ s}^{-1}$).

Taking heat capacity of peridotite:

$$C_p = 1150 \text{ J kg}^{-1} \text{ } ^\circ\text{C}^{-1};$$

Heat of fusion of peridotite:

$$H = 8.6 \times 10^5 \text{ J kg}^{-1}$$

Temperature increase:

$$\delta T = 1200 \text{ } ^\circ\text{C}$$

The thermal energy (Q) required to melt 1 kg of peridotite according to Eq. (4) is:

$$\begin{aligned} Q &= C_p(\delta T) + HQ = 1150 \text{ Jkg}^{-1} \text{ } ^\circ\text{C}^{-1}(1200 \text{ } ^\circ\text{C}) \\ &\quad + 8.6 \times 10^5 \text{ Jkg}^{-1} \\ &= 2.24 \times 10^6 \text{ Jkg}^{-1}. \end{aligned} \quad (4)$$

A magnitude-7 mantle earthquake at these conditions may therefore melt ca 63.6 kg peridotite per m^2 of the fault plane, corresponding to ca 2 cm thick layer of ultramafic pseudotachylyte. This estimate is considered to be a reasonable based on the field observations where 1–3 cm-thick pseudotachylyte fault veins are common. The heat of fusion (H) for peridotite is not well determined. Here we use a value of H for olivine given by [44] and a stress of 300 MPa in the calcu-

lation. This is close to an order of magnitude higher than stress-drops commonly measured by seismology [9]. The high stress value was chosen from a minimum estimate based on paleopiezometric measurements in the seismically faulted Balmuccia peridotite, where a stress of 3–600 MPa was obtained from detailed micro-textural studies of olivine dislocation-densities and olivine re-crystallized grain size distribution [5,6]. Extremely high stresses are also implied by the system of apparently conjugate fault veins (Fig. 3) and the high-pressure mineralogy of the pseudotachylytes [25]. We therefore prefer the high stress values derived from the combined geological/mineralogical criterion rather than those suggested by seismology. Alternatively, if the stresses were closer to those suggested from seismology, the near complete melting of peridotite would require larger displacement (closer to 10 m rather than 1 m suggested here) at lower stresses, implying much larger magnitude-9 earthquakes. It is suggested that several magnitude 7 or larger paleo-earthquakes generated the common 1–3 cm-thick pseudotachylyte fault veins in a close to conjugate fault system preserved in the mantle peridotite at Cima di Gratera.

6. Relationships between co-seismic slip, ductile fabric and metamorphism

It follows from the descriptions and interpretations above that co-seismic faulting at blueschist facies produced pseudotachylytes in the studied mantle rocks. The brittle faulting was in general a precursor to ductile deformation, although pseudotachylytes cutting small-scale shear zones and foliations can be observed (Fig. 5f). Pseudotachylytes were only generated in rocks retaining their mechanical framework supported by pyroxene and olivine (+plagioclase in gabbro). The ductile ultramafic rocks are dominated by serpentine, requiring introduction of vast quantities of water to form ($\sim 100 \text{ g H}_2\text{O kg}^{-1}$). Similarly, hydrous minerals including amphibole, epidote and sheet-silicates characterize the foliated mafic rocks. In detail, the better-preserved rocks with pseudotachylytes also display evidence of minor hydration predating generation of pseudotachylyte and ultra-cataclastite (Fig. 5f) [25]. Serpentine micro-veins and/or grain-boundary alteration textures have been observed in the wall rocks of pseudotachylyte. Previously described textures within pseudotachylyte veins from the gabbro also show replacement of *ortho*-pyroxene by talc prior to pseudotachylyte formation, and frictional heating in ultra-cataclastite associated with pseudotachylyte veins has

dehydrated serpentine to olivine (see Fig. 3 in [25]). If co-seismic faults truncated zones of serpentinisation, significant volumes of water may have been released by the dehydration reaction of serpentine to olivine [25,45]. Release of water may in turn have caused new seismic events by reducing the effective stress and may potentially have created swarms of earthquakes similar to those related to the release of CO_2 [46]. Indeed multiple events generating pseudotachylyte are common in all fault vein complexes observed in the present study.

The relationship and interdependence between frictional heating releasing water by dehydration reactions, frictional melting and hydration reactions related to ductile deformation may be more complicated. Evidence for dehydration reactions has so far only been observed at a small-scale in our previous study [25]. If seismic faults produce frictional melts, the water released may have been dissolved in the melt since silicate melts may contain very large amounts of water at high pressure [41]. It is therefore possible that significant frictional melting may reduce rather than increase local fluid pressure, whereas frictional faulting without melting may release water and increase the local fluid pressure. In spite of the limited observation of frictional-heat driven dehydration textures we suggest that local frictional heating may be a potentially important water-release mechanism in serpentine bearing rocks for reducing the strength and to trigger earthquakes.

7. Conclusions

The field, micro-textural and mineralogical data presented here documents that large paleo-earthquakes (magnitude-7 or larger?), from the Alpine HP-LT complex in Corsica resulted in common frictional fusion in both gabbro and mantle peridotite. The frictional heating on co-seismic faults in peridotite resulted in near complete disequilibrium melting, and raised the temperature by more than $1200 \text{ }^\circ\text{C}$ to over $1650 \text{ }^\circ\text{C}$. Microphenocrysts of olivine, *ortho*-, and clino-pyroxene and spinel crystallized directly from the friction melts, and veins thicker than $\sim 5 \text{ mm}$ commonly have acicular clinopyroxene forming radiating single crystals or disorder dendrites, which may have idiomorphic crystal habit adjacent to vesicles. This demonstrates that microphenocrysts crystallized directly from the melt and were not formed by later devitrification of a solidified glass. Solutions of Eq. (3) show that mm-thin veins solidified in seconds, whereas thicker melt pockets and veins ($> 2 \text{ cm}$) may have preserved liquid cores for minutes, hours

and in some cases days (38 cm thick vein solidified in ca 33 h). The characteristic fault-vein thicknesses, the mineralogy and micro-textures of the pseudotachylyte veins developed in a conjugate fault system within peridotites at blueschist facies pressure conditions suggest that the stress associated with the faulting was extremely high; alternatively the displacement and the paleo-earthquakes must have been much larger than magnitude-7.

Even though the co-seismic fault products are only preserved in the least hydrated rocks of the subduction complex, it is important to note that all the studied rocks preserve evidence of some earlier serpentinisation. Micro-porosity and chemical analyses of the mostly devitrified (?) interstitial matrix show that the fluid content of the ultramafic melt was up to 4%. The generation of pseudotachylyte may dehydrate wall rocks, whereas shear heating on seismic slip-zones without melting may release fluids by localized shear-heat-driven prograde reactions [25,45]. This may in turn locally lower effective stresses and trigger swarms of new co-seismic slip-events [46]. Frictional heating on shear zones and faults may therefore be important for seismic stress-release in adjacent drier rocks. Carefully designed studies are necessary to further assess and quantify the feedback mechanism between ductile deformation and earthquakes at HP-LT metamorphic conditions such as those prevailing in subduction zones.

Acknowledgements

A centre of excellence grant (SFF) to PGP from the Norwegian Research Council supported this study. Analyses were carried out at UiO and UCSB during a sabbatical of one of us (TBA). B. Hacker and M. Erambert are thanked for assistance with the analyses. D. Schmid wrote a matlab-script used in image analyses. We thank L. Jolivet and anonymous reviewer for their improvements and C. Marfisi and the staff at Kalliste for support in Corsica.

References

- [1] S.H. Kirby, Intermediate-depth intraslab earthquakes and arc volcanism as physical expressions of crustal and uppermost mantle metamorphism in subducting slabs, *Geophys. Monogr.* 96 (1996) 195–213.
- [2] A. Rietbrock, F. Waldhauser, A narrowly spaced double-seismic zone in the subducting Nazca plate, *Geophys. Res. Lett.* 31 (2004) L10608, doi:10.1029/2004.GL019610.
- [3] B.R. Hacker, S.M. Peacock, G.A. Abers, S. Holloway, Subduction factory 2. Are intermediate-depth earthquakes in subduction slabs linked to metamorphic dehydration reactions? *J. Geophys. Res.* 108 (2003), doi:10.1029/2001JB001129.
- [4] L. Jolivet, C. Faccenna, B. Goffé, E. Burov, P. Agard, Subduction tectonics and exhumation of high-pressure metamorphic rocks in the Mediterranean orogens, *Am. J. Sci.* 303 (2003) 353–409.
- [5] M. Obata, S.I. Karato, Ultramafic pseudotachylyte from the Balmuccia peridotite, Ivrea–Verbano zone, northern Italy, *Tectonophysics* 242 (1995) 313–328.
- [6] D. Jin, S.I. Karato, M. Obata, Mechanism of shear localization in continental lithosphere: inferences from the deformation microstructures of peridotites from the Ivrea zone, northwestern Italy, *J. Struct. Geol.* 20 (1998) 195–209.
- [7] T. Morishita, Possible pseudotachylyte from the Horoman peridotite complex of the Hidaka belt, Hokkaido, northern Japan, *J. Geol. Soc. Jpn.* 104 (1998) 18–23.
- [8] M.G. Lund, Metamorphism, earthquakes and fracturing of the deep continental crust, Unpubl. PhD, Univ. Oslo (2002) 169 pp.
- [9] S.C. Scholz, *The Mechanism of Earthquakes and Faulting*, Cambridge University Press, 1990, 439 pp.
- [10] J.G. Spray, Pseudotachylyte controversy: fact of friction?, *Geology* 12 (1995) 1119–1122.
- [11] H.R. Wenk, L.E. Weiss, Al-rich calcic pyroxene in pseudotachylyte: an indicator of high pressure and high temperature? *Tectonophysics* 84 (1982) 329–341.
- [12] G. Di Toro, D.L. Goldsby, T.E. Tullis, Friction falls to zero in quartz rock as slip velocity approaches seismic rates, *Nature* 427 (2004) 436–439.
- [13] H.R. Wenk, L.R. Johnson, L. Ratschbacher, Pseudotachylytes in the Eastern peninsular ranges of California, *Tectonophysics* 321 (2000) 253–277.
- [14] A. McGarr, On relating apparent stress to the stress causing earthquake fault slip, *J. Geophys. Res.* 104 (B2) (1999) 3003–3011.
- [15] K. Mair, C. Marone, Shear heating in granular layers, *Pure Appl. Geophys.* 157 (2000) 1847–1866.
- [16] M.A. d'Alessio, A.E. Blythe, R. Bürgmann, No frictional heat along the San Gabriel fault, California: evidence from fission-track thermochronology, *Geology* 31 (2003) 541–544.
- [17] C.H. Scholz, A fault in the weak San Andreas' theory, *Nature* 406 (2000) 234.
- [18] D.M. Saffer, B.A. Bekins, S. Hickman, Topographically driven groundwater flow and the San Andreas heat flow paradox revisited, *J. Geophys. Res.* 108 (B5) (2003) 2274, doi:10.1029/2002JB001849.
- [19] V.M. Goldschmidt, Om friksjonsglass (pseudo-tachylitt) i fjellkjeden, *GFF* 65 (1943) 83–84.
- [20] D.P. McKenzie, J.N. Brune, Melting of fault planes during large earthquakes, *Geophys. J. R. Astron. Soc.* 29 (1972) 8053–8068.
- [21] R.H. Sibson, Generation of pseudotachylyte by ancient seismic faulting, *Geophys. J. R. Astron. Soc.* 43 (1975) 775–794.
- [22] J.G. Spray, Artificial generation of pseudotachylyte using friction welding apparatus: simulation of melting on a fault plane, *J. Struct. Geol.* 9 (1987) 49–60.
- [23] J.F. MacLoughlin, J.G. Spray, Frictional melting processes and products in geological materials: introduction and discussion, *Tectonophysics* 204 (1992) 197–206.
- [24] H. Kanamori, D.L. Anderson, T.H. Heaton, Frictional melting during the rupture of the 1994 Bolivian earthquake, *Science* 279 (1998) 839–842.
- [25] H. Austrheim, T.B. Andersen, Pseudotachylytes from Corsica, fossil earthquakes from a subduction complex, *Terra Nova* 16 (2004) 193–197.

- [26] M. Fournier, L. Jolivet, B. Goffe, R. Dubois, Alpine Corsica Metamorphic core complex, *Tectonics* 10 (1991) 1173–1186.
- [27] D. Lahondère, Les schistes bleus et les eclogites a lawsonites des unites continentales et oceanques de la Corse alpine, Orleans, France, Bureau de Recherches Geol. et Minières, Doc., vol. 240, 1996, 285 pp.
- [28] D. Lahondère, D. Guerrot, Datation Sm–Nd du métamorphisme eclogitique en Corse alpine: un argument pour l'existence au Crétacé supérieur d'une zone de subduction active localisée sous le bloc Corso–Sarde, *Geol. Fr.* 3 (1997) 3–11.
- [29] R. Tribuzio, F. Giacomini, Blueschist facies metamorphism of peralkaline rhyolites from the Tenda crystalline massif (northern Corsica): evidence for involvement in the Alpine subduction event?, *J. Metamorph. Geol.* 20 (2002) 513–526.
- [30] E.J. Essene, Relatively pure jadeite from a siliceous Corsican gneiss, *Earth Planet. Sci. Lett.* 5 (1969) 270–272.
- [31] C. Brunet, P. Monié, L. Jolivet, J.P. Cadet, Migration of compression and extension in the Tyrrhenian Sea, insights from $^{40}\text{Ar}/^{39}\text{Ar}$ ages on micas along a transect from Corsica to Tuscany, *Tectonophysics* 321 (2000) 127–155.
- [32] J. Warburton, The ophiolite-bearing Schistes lustrés nappe in the Alpine Corsica: a model for the emplacement of ophiolites that have suffered HP/LT metamorphism, *Geol. Soc. Am. Mem.* 164 (1986) 313–331.
- [33] D. Lahondère, Eclogitic metamorphism in Farinoles orthogneisses and ophiolitic metabasites (Northern Corsica, France), *Bull. Soc. Geol. Fr.* 4 (1988) 579–585.
- [34] H. Austrheim, T.M. Boundy, Pseudotachylytes generated during seismic faulting and eclogitization of deep crust, *Science* 265 (1994) 82–83.
- [35] M.G. Lund, H. Austrheim, High-pressure metamorphism and deep-crustal seismicity: evidence from contemporaneous formation of pseudotachylytes and eclogite facies coronas, *Tectonophysics* 372 (2003) 59–83.
- [36] M.G. Björnerud, H. Austrheim, M.G. Lund, Processes leading to eclogitization (densification) of subducted and tectonically buried crust, *J. Geophys. Res.* 107 (2002), doi:10.1029/2001JB000527.
- [37] A. Suzuki, and collaborators, Viscosity of komatiite magma at high pressure, Bayerisches Geoinstitut Annual Report, 2001 http://www.bgi.uni-bayreuth.de/annual_report/navigat.php3?year=2001.
- [38] D.L. Turcotte, G. Schubert, *Geodynamics*, Cambridge University Press, 2002, 472 pp.
- [39] D.H. Lindsley, Pyroxene thermometry, *Am. Mineral.* 68 (1983) 477–493.
- [40] E. Stolper, D. Walker, Melt density and the average composition of basalt, *Contrib. Mineral. Petrol.* 74 (1980) 7–12.
- [41] B.O. Mysen, K. Wheeler, Solubility behavior of water in haploandesitic melts at high pressure and high temperature, *Am. Mineral.* 85 (2000) 1128–1142.
- [42] R.F. Katz, M. Spiegelman, C.H. Langmuir, New parameterization of hydrous mantle melting, *Geochem. Geophys. Geosyst.* 4 (2003) 1073, doi:10.1029/2002GC000433.
- [43] M.G. Bonilla, R.K. Mark, J.L. Lienkaemper, Statistical relations among earthquake magnitude, surface rupture length and surface fault displacement, USGS Open File Report 84–256, 1984 <http://geopubs.wr.usgs.gov/open-file/of84-256/>.
- [44] R.S. Bradley, Thermodynamic calculations on phase equilibria involving fused salts: Part II. Solid solutions and the application to the olivines, *Am. J. Sci.* 260 (1962) 550–554.
- [45] B. Wunder, W. Schreyer, Antigorite: high-pressure stability in the system MgO–SiO₂–H₂O (MSH), *Lithos* 41 (1997) 213–227.
- [46] S.A. Miller, C. Collettini, L. Chiaraluce, M. Cocco, M. Barchi, B.J.P. Kaus, Aftershocks driven by a high-pressure CO₂ source at depth, *Nature* 427 (2004) 724–727.
- [47] R. Kretz, Symbols for rock-forming minerals, *Am. Mineral.* 68 (1983) 277–279.